



ELSEVIER

Available online at www.sciencedirect.com

SCIENCE @ DIRECT®

Journal of Magnetism and Magnetic Materials 264 (2003) 146–152

Journal of
magnetism
and
magnetic
materials

www.elsevier.com/locate/jmmm

Exchange bias in a thin film dispersion of MnO nanocrystallites in Co

J. van Lierop^{a,*}, M.A. Schofield^a, L.H. Lewis^a, R.J. Gambino^b

^a *Materials Science Department, Brookhaven National Laboratory, Upton, NY 11973-5000, USA*

^b *Department of Materials Sciences and Engineering, State University of New York at Stony Brook, Stony Brook, NY 11794-2275, USA*

Received 29 November 2002

Abstract

Unusually large magnetization loops shifts along the field axis, of the same order as those observed in the archetypical exchange biased system Co/CoO, have been measured in a Co/MnO thin film made using reactive ion beam assisted deposition. These large loop shifts are unexpected for a system with an antiferromagnetic anisotropy that is two orders of magnitude less than that of CoO. This magnetic behavior is attributed to the nanoscale nature of the crystallites that constitute the film, where the surface area to volume ratio is large enough so that a sizable surface magnetic contribution provides the necessary antiferromagnet to ferromagnet coupling for the large measured exchange bias.

© 2003 Elsevier Science B.V. All rights reserved.

PACS: 75.30.Et; 75.70.Cn; 75.75.+a

Keywords: Exchange bias; Thin film; Nanocrystal

1. Introduction

Exchange coupling between the common interface of a ferromagnet and antiferromagnet leads to unidirectional anisotropy, commonly observed as a loop shift (H_E) of the magnetization curve away from the zero field axis. This loop shift is believed to stem from order in the antiferromagnet being established in the presence of the ferromagnet. The antiferromagnet is weakly coupled to external

fields so that its magnetization retains its direction even when the ferromagnet's magnetization is later rotated. The torque at the interface results in the loop shift, referred to as exchange bias [1–3].

Thin films of MnO nanocrystallites dispersed in nanocrystalline Co were deposited using the unique sample preparation technique of reactive ion beam assisted deposition (RIBAD) [4] from a target of nominal composition $\text{Co}_{96}\text{Mn}_4$. RIBAD uses a focused Ar ion beam from a deposition source to sputter metal atoms from a target onto a substrate surface while simultaneously a second ion beam from an assist source produces a controlled O_2/Ar mix beam. The sputtered metal becomes supersaturated with oxygen resulting in

*Corresponding author. Department of Physics, University of Michigan 500 E. University Avenue, Ann Arbor 48109, USA. Tel.: +7346479567; fax: +7347646843.

E-mail address: johanvl@umich.edu (J. van Lierop).

the precipitation of the oxide phase via nucleation and diffusion. By controlling the O₂/Ar mix, the Mn can be oxidized in preference to the Co [5]. Magnetometry studies indicate that unusually large loop shifts occur in this system (similar to those observed in the archetypical exchange biased system Co/CoO) for films deposited with an assist beam mix ratio greater than 5% O₂/Ar as shown in Fig. 1.

Typically, the interface coupling responsible for exchange bias is observed in systems where the ferromagnet's Curie temperature (T_C) is greater than the antiferromagnet's Néel temperature (T_N). Exchange bias occurs when the material is field-cooled from above T_N to a temperature (called the blocking temperature, T_B) where thermal effects no longer dominate over exchange effects, resulting in a shift, $H_E > 0$, of the hysteresis loop. Simple intuitive models, as well as more sophisticated theories, indicate the magnitude of H_E tracks with the size of the antiferromagnetic magnetocrystalline anisotropy, K_{AF} , such that $H_E = \frac{2}{M_F t_F} \sqrt{(J_{AF} K_{AF})} / a$ where M_F and t_F are the ferromagnet's saturation magnetization and thickness, J_{AF} the antiferromagnet's exchange constant, and a its lattice parameter

[2,3,6–8]. This expression reflects the measured trend of increasing H_E with decreasing ferromagnet layer thickness or crystallite size [3], although the linear dependence of H_E on the antiferromagnet thickness is not directly accounted for. Exchange bias theory, however, correctly predicts a linear dependence of H_E with temperature [2,8].

The large H_E values in the Co/MnO system are counterintuitive when we consider that the large H_E values in Co/CoO systems have been attributed to the high antiferromagnetic anisotropy compared with other exchange biased systems [2,3]. However, it is clear from comparing the magnetocrystalline anisotropy of CoO [9,10,2] ($K_{AFM} = 6 - 2 \times 10^5$ erg/cm³) to that of MnO [11] ($K_{AFM} = 6 \times 10^3$ erg/cm³) that the large H_E values we measure are inconsistent with the idea that H_E simply tracks with K_{AFM} . Furthermore, for %O₂/Ar mix ratios $x > 5$, H_E no longer exhibits a linear dependence with temperature (Fig. 1), and $T_B > T_N$. These remarkable results appear to be due in part to the unique geometry of these thin-film systems, i.e. nanometer sized antiferromagnetic crystallites embedded in a matrix of nanometer sized ferromagnetic crystallites, that is in contrast to the usual planar interface of layered systems. Additionally, a marked decrease in MnO crystallite size with $x > 5$ results in an increase in the ratio of surface area to volume and a concomitant increase in the number of uncompensated interfacial spins [2,12], providing the large number of antiferromagnet to ferromagnet couplings necessary for the large observed H_E .

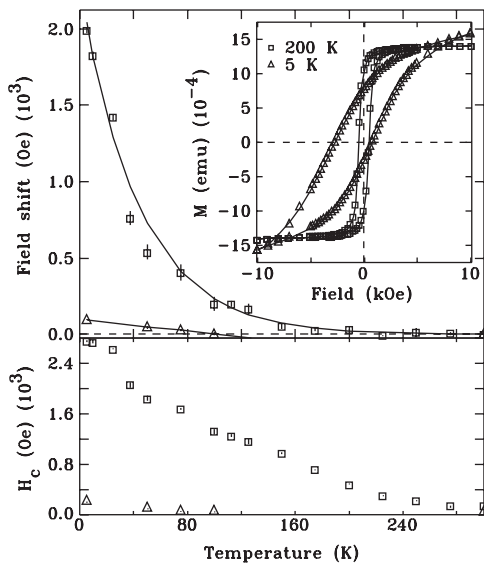


Fig. 1. Field shift and coercivity (H_c) as a function of temperature for the Co₉₆Mn₄ + 6%O₂/Ar film (□) and the Co₉₆Mn₄ + 2%O₂/Ar film (△). Inset shows typical magnetization loops for the Co₉₆Mn₄ + 6%O₂/Ar film at 200 K (□) and 5 K (△).

2. Experimental methods

The RIBAD system [13] used two ion sources and gas lines for mixing of the process gases (Ar and O₂) with a backside water-cooled target of 150 mm diameter, 6 mm thick Co (99.999% pure) that had an array of 6 mm diameter Mn pellets made by sintering commercial 300 mesh Mn powder (99.99%) in a 4% H/Ar gas mix. The area ratios were set so that a nominal composition of Co₉₆Mn₄ resulted. After an initial pump-down to $\sim 10^{-5}$ Pa, all films were deposited on backside water-cooled single crystal Si substrates that were

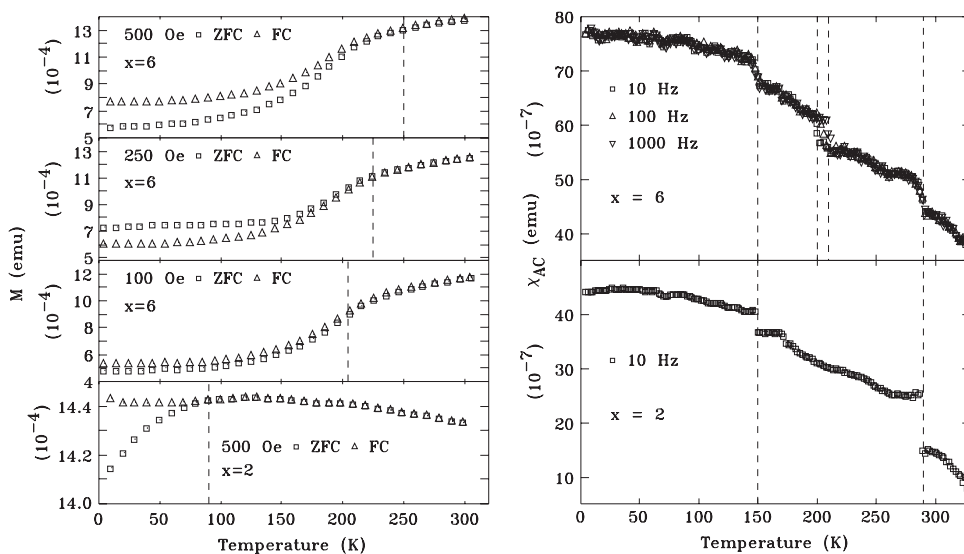


Fig. 2. Left: ZFC (\square) and FC (\triangle) magnetization (M) vs. temperature for the $\text{Co}_{96}\text{Mn}_4 + 2\% \text{O}_2/\text{Ar}$ film (bottom panel) and $6\% \text{O}_2/\text{Ar}$ film. Right: χ_{AC} versus temperature data for the $2\% \text{O}_2/\text{Ar}$ film (bottom panel) and $6\% \text{O}_2/\text{Ar}$ film (top panel).

sputter cleaned and rotated during deposition at a 30° tilt with respect to the target. With the deposition chamber at $\sim 10^{-1}$ Pa, a bias voltage of 700 eV and drive current of 200 mA were used for the ion sources. Samples of approximately $5 \times 5 \text{ mm}^2$ pieces of film with a 50 nm average thickness, determined with an α -step surface profiler, were examined using a commercial SQUID magnetometer. Magnetization data were collected in fields up to 50 kOe, and AC susceptibility (χ_{AC}) data were collected in 10, 100 and 1000 Hz oscillating fields of 3.5 Oe. Cu K_α X-ray diffraction (XRD) was used to characterize sample phase composition and crystallite sizes. Transmission electron microscopy (TEM) and electron energy loss spectroscopy (EELS) were performed on films deposited on TEM grids positioned next to substrates during film deposition. Auger electron spectroscopy (AES) was used to confirm elemental composition and depth profiling the films. We describe results on films deposited with assist beam mix O_2/Ar ratios of $x = 2$ and 6% .

3. Results and discussion

Typical magnetization curves for the $\text{Co}_{96}\text{Mn}_4 + 6\% \text{O}_2/\text{Ar}$ film as well as the coercivity

(H_C) and field shift as a function of temperature for both $\text{Co}_{96}\text{Mn}_4 + 2\% \text{O}_2/\text{Ar}$ and $6\% \text{O}_2/\text{Ar}$ films are shown in Fig. 2. The samples were zero field-cooled from 300 K to the measuring temperature. Examining the loop-shift values for the $\text{Co}_{96}\text{Mn}_4 + 2\% \text{O}_2/\text{Ar}$ ($x = 2$) film, we measure the expected H_E values considering the low K_{AFM} of MnO. $H_E > 0$ at temperatures below 100 K, consistent with a $T_B \sim 90$ K that is marked by the temperature where the zero field-cooled (ZFC) and field-cooled (FC) magnetization separate with decreasing temperature [12,14], shown in Fig. 2. A $T_N \sim 150$ K for the MnO is indicated by the χ_{AC} measurements (Fig. 2). XRD and TEM electron diffraction data indicate the film is composed of both FCC and HCP Co and MnO, with no evidence of CoO or CoMnO compounds in the bulk of the film. Measured L_3/L_2 ionization edge area ratios from the EELS data of 2.67 ± 0.29 and 3.41 ± 0.30 are also consistent with Co and MnO, respectively [15,16]. AES data indicates a CoO oxide layer on the surface of the film that is 2–5 nm thick, in good agreement with the expected passive oxide layer of Co [17] and is also seen in the χ_{AC} data of Fig. 2 ($x = 2$) where $T_N \sim 290$ K. Scherrer analysis of the XRD peaks indicate Co crystallite sizes of 12.3 ± 1.3 nm and MnO crystallite sizes of 14.8 ± 1.1 nm, in agreement with TEM images.

On the other hand, the $\text{Co}_{0.96}\text{Mn}_4 + 6\% \text{O}_2/\text{Ar}$ ($x = 6$) film marks $H_E > 0$ below 200 K. A T_B of around 200 K is denoted by the separation point of the ZFC and FC 100 Oe magnetization data (Fig. 2). Additional evidence that this marks a blocking temperature rather than a magnetic transition temperature (e.g. T_N) is denoted by the shift of the ZFC/FC separation temperature with increasing bias field, shown in Fig. 2, consistent with the blocking temperature behavior of nanocrystallite and single-domain particles [12]. Further confirmation of blocking behavior about this temperature range is given by the frequency dependence of the temperature when a slope change occurs in the χ_{AC} data shown in Fig. 2 around 200 K, in contrast to the frequency independent changes marking T_N . Likewise, similar to the $x = 2$ film, a $T_N \sim 150$ K of the MnO is indicated in the χ_{AC} data of the $x = 6$ film in Fig. 2. XRD and TEM electron diffraction data indicate the film is composed of both fcc and hcp Co and MnO. Measured L_3/L_2 ionization edge area ratios from the EELS data of 2.80 ± 0.23 and 3.60 ± 0.27 , also consistent with Co and MnO, respectively [2–5]. AES data indicates a CoO oxide layer on the surface of the film that is 2–5 nm thick, similar to the $x = 2$ film. XRD Scherrer analysis and TEM images (Fig. 3) indicate Co crystallite sizes of 6.1 ± 0.5 nm and MnO crystallite sizes of 7.7 ± 0.5 nm. Fig. 4 shows the saturation magnetization (M_s) as a function of temperature for the $x = 6$ film. The fitted solid line is in good agreement with $M_s(T)$ of Co, and the amounts of Co and Mn calculated from $M_s(300$ K) are in accord with the AES data and target configuration. The increase of M_s at temperature below ~ 100 K signifies a large surface magnetic contribution from the crystallites [12,18].

To understand the differences between the two films, we see that for the $\text{Co}_{0.96}\text{Mn}_4 + 2\% \text{O}_2/\text{Ar}$ film the usual situation for an exchange biased material exists [2,3]. That is, T_B (~ 90 K) is lower than T_N (~ 150 K) of the MnO (Fig. 2) and $H_E > 0$ below T_B . Since the magnetic coherence length goes as $1/(T - T_C)^n$ where $n \sim \frac{1}{2}$ [19], and $T_C = 1388$ K [20], at the temperatures where $H_E > 0$ the assumption that the crystallite size is representative of the depth to which magnetic coupling can

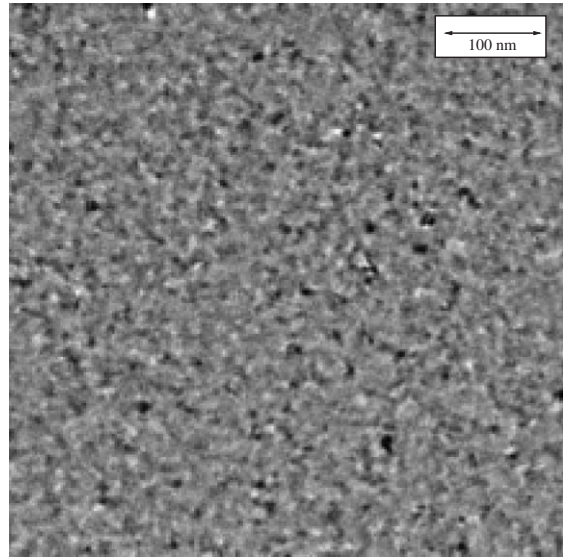


Fig. 3. Typical TEM brightfield image of $\text{Co}_{95}\text{Mn}_4 + 6\% \text{O}_2$ film at 40kX.

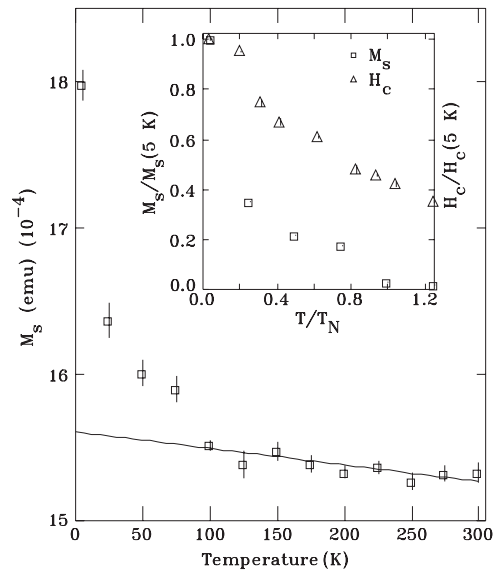


Fig. 4. Saturation magnetization (M_s) versus temperature for the $\text{Co}_{96}\text{Mn}_4 + 6\% \text{O}_2/\text{Ar}$ film ($H_{\text{max}} = 30$ kOe). Inset shows the normalized M_s and H_c as a function of T/T_N .

occur seems reasonable. For a rough estimate (as the film geometry is not planar), if we take the Co crystallite size to be representative of the

ferromagnet thickness, and using published values of J_{AF} [21], K_{AF} [11] and M_F at 5 K (Fig. 4) [20], we find that $H_E \sim 80$ Oe, in good agreement with $H_E(5\text{ K}) = 95 \pm 4$ Oe. The situation is very different for the $\text{Co}_{96}\text{Mn}_4 + 6\% \text{O}_2/\text{Ar}$ film, T_B is higher than T_N (Fig. 2), unusual for an exchange biased material. Furthermore, using the same mean-field argument for the magnetic coherence length, and confirming this argument with an estimation of the MnO nanocrystallite density from $M_s(300\text{ K})$ that substantiates the approximation that the Co nanocrystallite size can represent the ferromagnet thickness, we find $H_E \sim 130$ Oe at 5 K, in stark contrast to the measured $H_E = 1992 \pm 18$ Oe.

Clear evidence of the much stronger exchange bias in the $\text{Co}_{96}\text{Mn}_4 + 6\% \text{O}_2/\text{Ar}$ ($x = 6$) film compared to that of the $\text{Co}_{96}\text{Mn}_4 + 2\% \text{O}_2/\text{Ar}$ ($x = 2$) film is shown by the temperature dependence of the magnetization (Fig. 2). For the $x = 2$ film, field cooling (FC) in a 500 Oe field is enough to substantially change the low temperature $M(T)$ compared to the ZFC $M(T)$, until enough thermal energy is present to overcome the unidirectional exchange anisotropy, marking T_B . For the $x = 6$ film, due to the much stronger unidirectional exchange anisotropy [14], the perturbative fields have small effect (compared to the $x = 2$ film) on the low-temperature ZFC and FC results, as shown by $M(T)$ remaining basically unchanged up to ~ 100 K.

Initially, one might suppose that the large H_E values observed in the $x = 6$ film is due to the passive CoO layer on the surface of the film since CoO has a sufficiently high K_{AFM} to account for $H_E(T)$. However, both films have the same thickness of surface CoO according to the AES depth profiling results, yet the $x = 2$ film does not exhibit anomalously high H_E values. Moreover, the EELS data, which is exquisitely sensitive to differences in ionization edge energies and provides a measure of the oxidation state of the Co in the whole film, shows the same Co L_3/L_2 edge ratios between the $x = 2$ and $x = 6$ films, indicating that the nature of the Co oxide is the same in both films. This consistent Co L_3/L_2 edge ratio between the two films is strong evidence that the $x = 6$ film has not formed other Co mixtures such as CoMnO relative to the $x = 2$ film that could

explain the anomalous H_E values. Furthermore, XRD data only shows evidence of Co and MnO in both $x = 2$ and $x = 6$ films, and the χ_{AC} data shows the same T_N for the MnO and surface CoO in both $x = 2$ and $x = 6$ films. If there was a significant difference in the phase compositions between the two films, T_N would be different, and it is not (Fig. 2).

The nanoscale nature of the Co and MnO crystallites is the likely cause for the exceptional magnetic behavior of the $x = 6$ film. For exchange biased materials with antiferromagnetic components smaller than ~ 10 nm [22], the size regime of the MnO nanocrystallites in the $x = 6$ film, enhanced T_N has been observed, corresponding the elevated $T_N \sim 150$ K (compared to the bulk $T_N \sim 120$ K [20]) of the MnO component, and is attributed to proximity effects from the ferromagnet component [22]. Also, an enhanced T_N has been seen in neutron diffraction studies of 7 nm MnO nanocrystallites where finite size effects cause collective spin freezing at the surface from competition between the exchange and anisotropy energies [23].

It is clear that the decrease in the average Co and MnO nanocrystallite size from the $x = 2$ to $x = 6$ film is responsible for the drastic change in magnetic exchange properties. The much stronger exchange coupling in the $x = 6$ film is mirrored in the $H_E(T)$ results shown in Fig. 1. While $H_E(T)$ is linear for the $x = 2$ film, standard exchange bias behavior [2], $H_E(T)$ is exponential for the $x = 6$ film (solid line in the $H_E(T)$ plot of Fig. 1 is a fit to an exponential) and around 20 times larger at low temperatures than in the $x = 2$ system. This Arrhenius-type behavior would indicate temperature-dependent moment fluctuations are driving the exchange coupling. Although H_E is known to increase with decreasing ferromagnet component thickness [2], in general H_E also decreases with decreasing antiferromagnet component thickness [2,3]. Since both components crystallite sizes decreased, presumably these effects were nullified. Nevertheless, if we examine the surface area to volume ratios of the MnO nanocrystallites (approximately 0.4 nm^{-1} for the $x = 2$ film and 0.75 nm^{-1} for the $x = 6$ film), for the $x = 6$ film (with large $H_E(T)$) there should be a greater

number of uncompensated interfacial spins [2]. Since the magnetic sublattices that constitute the antiferromagnetic crystallites cannot be exactly compensated due to the small size [12], this large number of interfacial spins allows stronger exchange bias. Basically, a large part of the magnetism in the film seems to be from surface contributions, where more ferromagnet to antiferromagnet coupling is possible with the increase of uncompensated surface spins. This is supported by the $T_B > T_N$ for the $x = 6$ film where the large number of surface interfacial spins, with decreasing temperature, begin to freeze at around ~ 200 K, and start to couple to the ferromagnetic component that results in weak exchange bias (denoted by the small H_E starting at 200 K in Fig. 1). As the film cools, more spins freeze and couple, resulting in stronger unidirectional anisotropy as shown by the strong increase of $H_E(T)$. With larger nanocrystallite sizes, the $x = 2$ film possesses a smaller number of surface spins, resulting in a smaller H_E that agrees with theory.

This increased surface spin contribution in the $x = 6$ film is also marked by the exponential-like increase of $M_s(T)$ at temperatures below ~ 100 K (Fig. 4) [18]. The normalized $M_s(T)$ for the MnO nanocrystallites as a function of reduced temperature ($T/T_{N=150\text{ K}}$) is shown in the inset of Fig. 4.¹ The magnetization versus temperature behavior in Fig. 4 is in good qualitative agreement with Monte Carlo simulations of uncompensated spins in antiferromagnetic nanoparticles with a z -axis core anisotropy and small radial surface anisotropy [24]. Additionally, the coercive field versus temperature behavior of the $x = 6$ film (shown in the inset of Fig. 4) is in good agreement with similar Monte Carlo simulations of exchange biased nanocrystallites with a small number of core spins and attendant large number of surface spins [25].

Subtracting the Co $M_s(T)$ values with a linear fit to the higher-temperature data where only Co is magnetized (the fitted line shows the expected

$\sim 4\%$ increase between $M_s(300\text{ K})$ to $M_s(5\text{ K})$ for Co [20]), the resulting normalized $M_s(T)$ for the MnO nanocrystallites as a function of reduced temperature ($T/T_{N=150\text{ K}}$) is shown in the inset of Fig. 4. The magnetization versus temperature behavior in Fig. 4 is in good qualitative agreement with Monte Carlo simulations of uncompensated spins in antiferromagnetic nanoparticles with a z -axis core anisotropy and small radial surface anisotropy [24]. Additionally, the coercive field versus temperature behavior of the $x = 6$ film (shown in the inset of Fig. 4) is in good agreement with similar Monte Carlo simulations of exchange biased nanocrystallites with a small number of core spins and attendant large number of surface spins [25].

In summary, a thin film dispersion of MnO nanocrystallites in Co demonstrate unusually large loop shifts when the component's crystallite size results in a large surface to area ratio with the consequence of a large surface magnetic contribution. This system is unique since it does not agree with the established trend of large H_E corresponding to large K_{AFM} . In this system, at low temperature, measured H_E is comparable to Co/CoO systems [3] that have a K_{AFM} that is two orders of magnitude larger [9,2] than the present system [11].

References

- [1] W.H. Meiklejohn, C.P. Bean, Phys. Rev. 105 (1957) 904.
- [2] A.E. Berkowitz, Kentaro Takano, J. Magn. Magn. Mater. 200 (1999) 552.
- [3] J. Nogués, I.K. Schuller, J. Magn. Magn. Mater. 192 (1999) 203.
- [4] J. van Lierop, L.H. Lewis, K.E. Williams, R.J. Gambino, J. Appl. Phys. 91 (2002) 7233.
- [5] CRC Handbook of Chemistry and Physics.
- [6] R.L. Stamps, J. Phys. D 33 (2000) R247.
- [7] M. Kiwi, J. Magn. Magn. Mater. 234 (2001) 584.
- [8] A.P. Malozemoff, Phys. Rev. B 35 (1987) 3679.
- [9] A.E. Hughes, Phys. Rev. B 3 (1971) 877.
- [10] A.J. Sievers, jrIII, M. Tinkham, Phys. Rev. 129 (1963) 1566.
- [11] F. Keffer, W. O'Sullivan, Phys. Rev. 108 (1957) 637.
- [12] J.L. Dormann, D. Fiorani, E. Tronc, in: I. Prigogine, S.A. Rice (Eds.), Advances in Chemical Physics, XCVIII, Wiley, New York, 1997, p. 283.

¹ $M_s(T)$ of the MnO component was calculated by subtracting the extrapolated Co $M_s(T)$ using a least-squared fit to high-temperature data where only Co is magnetized, from the measured $M_s(T)$ in Fig. 4. The fitted line shows the expected $\sim 4\%$ increase between $M_s(300\text{ K})$ to $M_s(5\text{ K})$ for Co [20].

- [13] K.E. Williams, Ph.D. Thesis, Materials Science and Engineering Department, State University of New York at Stony Brook, 2000.
- [14] D.L. Peng, K. Sumiyama, T. Hihara, S. Yamamuro, T.J. Konno, *Phys. Rev. B* 61 (2000) 3103.
- [15] M. De Crescenzi, J. Derrian, E. Chainet, K. Orumchian, *Phys. Rev. B* 39 (1989) 5520.
- [16] H. Kurata, C. Colliex, *Phys. Rev. B* 48 (1993) 2102.
- [17] R.P. Frankenthal, J. Kruger, *Passivity of Metals*, The Electrochemical Society, Inc., New Jersey, USA, 1973.
- [18] E. De Biasi, C.A. Ramos, R.D. Zysler, H. Romero, *Phys. Rev. B* 65 (2002) 144416.
- [19] H.E. Stanley, *Introduction to Phase Transitions and Critical Phenomena*, Oxford University Press, Oxford, 1971.
- [20] C. Kittel, *Introduction to Solid State Physics*, Wiley, New York, 1996.
- [21] T. Oguchi, K. Terakura, A.R. Williams, *Phys. Rev. B* 28 (1983) 6443.
- [22] P.J. van der Zaag, Y. Ijiri, J.A. Borchers, L.F. Feiner, R.M. Wolf, J.M. Gaines, R.W. Erwin, M.A. Verheijen, *Phys. Rev. Lett.* 84 (2000) 6102.
- [23] I.V. Golosovsky, I. Mirebeau, G. André, D.A. Kurdykov, Yu.A. Kumzerov, S.B. Vakhrushev, *Phys. Rev. Lett.* 86 (2001) 5783.
- [24] K.N. Trohidou, X. Zianni, J.A. Blackman, *J. Appl. Phys.* 84 (1998) 2795.
- [25] K.N. Trohidou, X. Zianni, J.A. Blackman, *Phys. Stat. Sol. A* 189 (2002) 305.